Positive and Negative Retinotopic Codes in the Human Hippocampus

Peter A. Angeli[1,6*], Adam Steel[1,2,3], Edward H. Silson[4], Caroline E. Robertson[1,5**]

[1] Department of Psychology, Dartmouth College, Hanover, NH, USA

[2] Beckman Institute, University of Illinois Urbana-Champaign, Urbana, IL, USA

[3] Department of Psychology, University of Illinois Urbana-Champaign, Urbana, IL, USA

[4] Department of Psychology, University of Edinburgh, Edinburgh, UK

[5] Senior Author

[6] Lead Contact

* Correspondence: peter.a.angeli@dartmouth.edu

** Correspondence: caroline.e.robertson@dartmouth.edu

Competing interest: The authors declare no competing interests.

Data availability: All raw and minimally processed data is made publicly available via the Natural Scenes Dataset (naturalscenesdataset.org). Subsequently analyzed data available from lead contact upon request.

Code availability: All analyses performed with publicly available code packages. Additional information needed for reanalysis or replication is available from the lead contact upon request.

Acknowledgements: The authors would like to thank the Natural Scene Dataset authors for making their data publicly available. This work was supported by funding from the National Institutes of Mental Health under award number R01MH130529 to CER, from the Neukom Institute for Computational Sciences to AS, and from the Biotechnology and Biological Sciences Research Council award BB/V003917/1 to EHS.

Number of Figures: 4

Number of Tables: 0

Number of Supplemental Figures: 6

Abstract Word Count: 186

Main Text + Figure Legend Word Count: 2262

Abstract

The hippocampus is thought to coordinate sensory-mnemonic information streams in the brain, representing both the apex of the visual processing hierarchy and also a central hub of mnemonic processing. Yet, the mechanisms underlying sensory-mnemonic interactions in the hippocampus are poorly understood. Recent work in cortex suggests that a retinotopic code – typically thought to be exclusive to visual areas – may help organize internal and external information at the cortical apex via opponent interactions. Here, we leverage high-resolution 7T functional MRI to test whether a bivalent retinotopic code structures activity within the human hippocampus, and mediates hippocampal-cortical interactions. Our findings reveal a robust retinotopic code in the hippocampus, characterized by stable population receptive fields (pRFs) with consistent preferred visual field locations across experimental runs. Notably, this retinotopic code comprises roughly equal proportions of positive and negative pRFs, aligning with the hypothesized role of negative pRFs in mnemonic processing. Finally, the signed amplitude of hippocampal pRFs predicts functional connectivity between retinotopic hippocampal and cortical voxels. Taken together, these results suggest that retinotopic coding may scaffold internal mnemonic and external sensory information processing within the hippocampus, and across hippocampal-cortical interactions.

Introduction

Classic views of the brain posit that sensory and mnemonic information occupy opposite poles of the visual processing hierarchy (Felleman and Van Essen 1991). As information ascends the visual hierarchy toward the hippocampus, it is thought that representations become progressively more memory-oriented, gradually shedding sensory-based neural codes such as retinotopy. However, recent findings challenge this view. Even in the hippocampus – at the apex of this hierarchy – signatures of egocentric sensory information processing, including retinotopy, appear to be more preserved than previously thought. For example, recent evidence for the coding of egocentric visual information has been found in the hippocampus of both rodents (Acharya et al. 2016; Purandare et al. 2022) and non-human primates (Gulli et al. 2020), while representations of the retinal position of visual stimuli have been found in the human hippocampus (Knapen 2021; Silson et al. 2021). These findings are particularly striking given the well-established role of the hippocampus in episodic memory (Scoville and Milner 1957; Cohen and Squire 1980) and potentially related abstract representations like allocentric spatial position (O'Keefe and Dostrovsky 1971). How might a retinotopic code support information-processing within this core memory structure?

A possible clue comes from recent studies describing retinotopic coding in memory-related cortical regions such as the default network (DN). In contrast to the positive response typically observed in visual regions, retinotopy in the DN is characterized by decreased activity during visual presentation (Szinte and Knapen 2020; Klink et al. 2021; Knapen 2021; Steel et al. 2024). Notably, this negative retinotopic response structures an opponent dynamic between mnemonic

regions within the DN and nearby perceptual regions containing positive retinotopic responses (Steel et al. 2024). This relationship suggests that retinotopic codes may help coordinate sensory-mnemonic interactions across cortical networks by “tagging” mnemonic vs. perceptual information streams at the cortical apex. Yet, to date, it is unknown whether this bivalent retinotopic code exists in the hippocampus, or how it might shape hippocampal-cortical interactions.

Here, we leverage high-resolution 7T functional MRI to test whether a bivalent retinotopic code structures activity within the human hippocampus and mediates hippocampal-cortical interactions. We tested two specific hypotheses. First, if positive and negative retinotopy correspond to perceptual and mnemonic information, respectively, we would expect negative retinotopic responses in the hippocampus, given its central role in episodic memory. Second, if positive and negative retinotopy support the separation of sensory and mnemonic information, we anticipate distinct whole-brain functional connectivity patterns for each type of hippocampal retinotopy.

In brief, our results show the hippocampus contains a robust retinotopic code, with a roughly equal proportion of positive and negative population receptive fields (pRFs) distributed evenly throughout the hippocampus. Critically, the signed response amplitude of a retinotopic hippocampal voxel (i.e. positive or negative) predicts its functional connectivity with retinotopic voxels across cortex, suggesting that a bivalent retinotopic code scaffolds information processing both within the hippocampus, and across hippocampal-cortical networks.

Results

The Hippocampus Contains Both Positive and Negative Visually Responsive Voxels

To interrogate the role positive and negative retinotopy plays in structuring perceptual and mnemonic information in the hippocampus, we first robustly characterized hippocampal retinotopy. In particular, while positive retinotopy has been previously described in the hippocampus (Knapen 2021; Silson et al. 2021), the extent of negative retinotopy remains unknown. To this end, we applied a population receptive field (pRF) modeling approach (Dumoulin and Wandell 2008) to interrogate hippocampal activity during a sweeping bar retinotopic mapping task (see Methods). Specifically, we used pRF modeling as implemented in AFNI (Cox 1996, 2012, see Silson et al. 2015; Steel et al. 2024), which critically allows for positive and negative amplitude parameters (Fig. 1A).

We observed both positive and negative retinotopic responses in the hippocampus, with some voxels displaying exceptional model fits (e.g. $R^2 > 0.4$, Fig. 1B). Pooled across all participants, the average goodness of fit (R^2) for hippocampal voxels was 0.083, with slightly stronger fits for negative amplitudes than positive (negative mean $R^2 = 0.086$, positive mean $R^2 = 0.081$; Welch two-sample t-test, $t(7110.5) = -4.612$, $p < 0.001$). For subsequent analyses, it was necessary to establish a goodness of fit threshold to separate robust, visually responsive voxels from voxels with models fit to noise. We established this threshold quantitatively by assessing goodness of

fit in a null model calculated from resting-state fixation. Fixation was an ideal null comparison because it lacked the dynamic visual stimuli the model expects, but also retained many other potential drivers of erroneous model fit such as auto-correlations and large-scale fluctuations in signal.

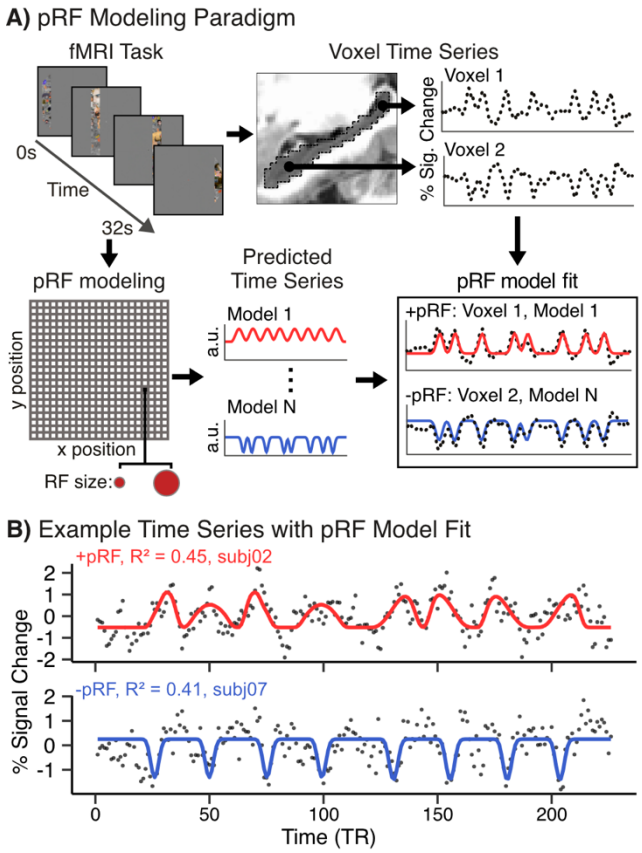

Fig. 1. *Population receptive field (pRF) modeling approach for identifying both positive and negative retinotopic responses in the hippocampus.* ***A.*** *Schematic of fMRI pRF modeling paradigm, starting with a sweeping bar visual mapping task, derived from the Human Connectome Project RETBAR task (top left, Benson et al. 2018). From task data, we modeled the predicted activity for 4 million possible pRFs, covering all possible combinations of x position, y position, and size. From these possible time series, the closest match was chosen for each voxel of observed data, with flexibility to apply an amplitude scalar (either positive, in red, or negative, in blue) to improve fit. Voxels with a positive amplitude parameter are termed +pRFs, while those with negative amplitude parameters are termed -pRFs.* ***B.*** *Example voxel time series with model fit highlight exceptional model fits in hippocampal voxels. Dots are observed time-points, solid line shows the best model fit. Note the increase in activation relative to baseline in the +pRF, in contrast to the -pRF's significant deactivation below baseline.*

Our analysis confirmed the presence of robust and reliable positive and negative pRFs in the hippocampus. In comparison to the fixation-derived null, pRF model fits on data from the

sweeping bar task explained significantly more variance in hippocampal activity (Fig. 2A; all *p*-values < 0.001), even when considering only positively or negatively responding voxels (all *p*-values < 0.05). Crucially, this allowed us to use the 95th percentile of the null model fit (R^2 = 0.117) as a threshold for task-based model fits (along with conservative screens for size and eccentricity, see Methods), identifying voxels with significant visual responses. These significantly responding voxels also demonstrated stable pRF features (Fig. 2B). Both center position estimates and signed response amplitude (i.e., positive or negative responses during the sweeping bar task) were highly reliable across single runs of the sweeping bar task (versus random samplings of all hippocampal voxels, see Methods; all center position *p*-values < 0.01; all signed response amplitude *p*-values < 0.05).

On average, 9% of hippocampal voxels displayed a significant pRF in response to the sweeping bar task. Interestingly, this proportion of significant pRFs is fairly close to the 13% of hippocampal neurons recently identified as showing a bidirectional sensitivity to the location of a moving light bar in body-fixed rats (Purandare et al. 2022). This both supports the validity of our significance thresholds and suggests a relatively consistent prevalence of visually-responsive hippocampal neurons across species.

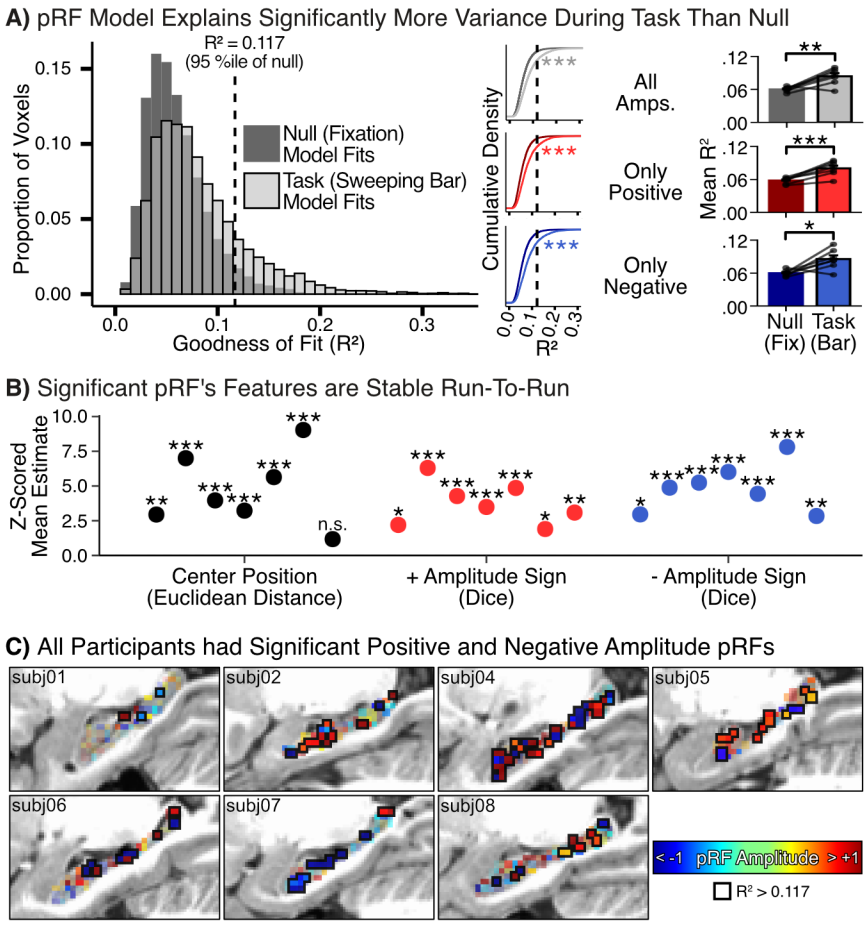

Fig. 2. *Hippocampal pRF modeling is reliable and robustly identifies both + and -pRFs across participants.* ***A.*** *The pRF model explains significantly more variance when fit on hippocampal*

activity during a sweeping bar task than when fit on null activity during resting-state fixation. Pooling hippocampal voxels across participants (left), the distribution of pRF model fits calculated on task data was significantly right shifted compared to those fit on null data (asymptotic two-sample Kolmogorov-Smirnov Test, H_a:task < null, all amplitudes: D- = 0.224, p < 0.001; positive amplitudes only: D- = 0.217, p < 0.001; negative amplitudes only: D- = 0.239, p < 0.001). The task-fit model also explained more variance on a participant level (right, paired t-test, all amplitudes: t(6) = 3.779, p < 0.001; positive amplitudes only: t(6) = 6.039, p < 0.001; negative amplitudes only: t(6) = 3.238, p < 0.05) ***B.*** *In hippocampal voxels that passed the significance thresholds, key pRF features (center position, amplitude) are consistent between individual runs of the retinotopic mapping task. Center position consistency was calculated using average Euclidian distance between pairs of runs (black dots), while amplitude sign was calculated using a 3-run Dice-like coefficient (red and blue dots). Significant voxel coefficients were compared against distribution of coefficients sampled from all hippocampal voxels. Each point is a participant, from left to right: subj01, subj02, subj04, subj05, subj06, subj07, and subj08.* ***C.*** *Representative maps of pRF modeling results for each participant. Across participants, 9% of hippocampal voxels displayed significant pRFs, and every participant had both positive and negative pRFs. Voxel opacity reflects magnitude of R^2 value, and voxels passing significance threshold of 0.117 are outlined. Error bars indicate standard error around the mean. ***p < 0.001 **p < 0.01 *p < 0.05*

Intriguingly, the hippocampus showed a balance of significant positive and negative visual responses (+pRFs and -pRFs). Every participant had both +pRFs and –pRFs in their hippocampus (Fig. 2C), and on average slightly over half (55%) of the significant hippocampal pRFs had a negative response amplitude. We also found a remarkably even spatial distribution within the hippocampus, with no significant difference in the prevalence of -pRFs (or significant pRFs more generally) along the long axis of the hippocampus (Supplemental Fig. 1) or between hippocampal subfields (Supplemental Fig. 2). This uniformity in both prevalence and spatial location indicates that retinotopically-scaffolded interactions may be relevant to a wide range of hippocampal functions.

Hippocampal pRFs are Consistent with Whole-Brain Retinotopic Organization

Placing the hippocampus within its context in the visual hierarchy strengthens the view the +pRFs pattern perceptual information while -pRFs organize mnemonic information, and is particularly clear along the ventral visual pathway (Fig 3). Early visual cortex is primarily driven by perceptual information and is dominated by +pRFs. Moving up the hierarchy, the proportion of -pRFs gradually increases, even while the overall proportion of significant pRFs decreases. Within the parahippocampal place area (PPA), the anterior portion implicated in scene memory (Steel et al. 2021, 2024) has a higher proportion of -pRFs than the posterior portion involved in scene perception (Epstein and Kanwisher 1998). This pattern culminates in the hippocampus, which has the highest proportion of -pRFs.

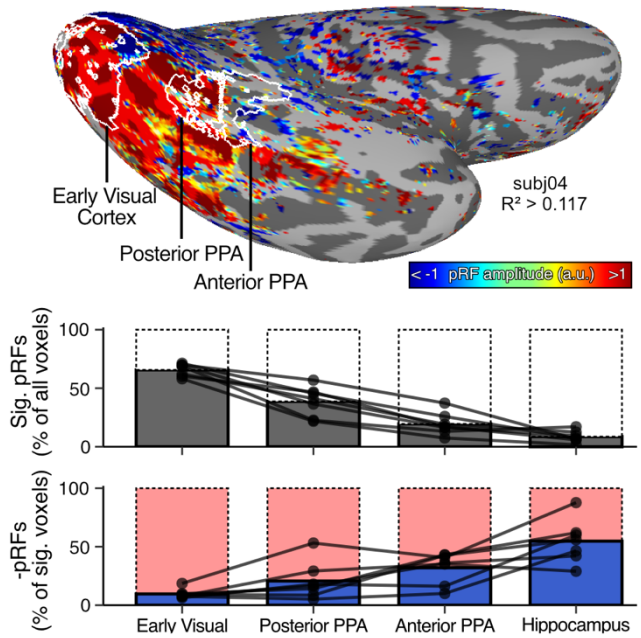

Fig. 3. *While pRF prevalence decreases along the visual hierarchy, the proportion of -pRFs increases.* ***Top.*** *Regions of interest displayed on the cortical surface over pRF amplitudes in an example participant highlights how pRF prevalence changes along the ventral visual stream.* ***Bottom.*** *Pooling across participants, -pRF prevalence increases moving up the visual hierarchy, despite a decreasing overall proportion of significant pRFs, culminating in the hippocampus with the fewest pRFs and highest proportion of -pRFs. ROIs for early visual cortex and PPA provided as part of NSD release. PPA split into anterior and posterior portions at center of mass. PPA = parahippocampal place area.*

If pRF signed response amplitude serves as a tag for sensory versus mnemonic information, then this feature should also be reflected in hippocampal-cortical connectivity more broadly: hippocampal +pRFs should primarily be connected to cortical +pRFs, while hippocampal -pRFs should primarily be connected to cortical -pRFs. Using hippocampal-cortical functional connectivity as a useful but limited proxy for anatomical connectivity (Fig. 4A, Biswal et al. 1995; Fox and Raichle 2007), we found that cortical pRFs are significantly more coupled to hippocampal pRFs which share the same sign response amplitude (Fig. 4B). The same-sign preference was present in both a simple correlation analysis (all p-values < 0.05) and a functional-connectivity derived ROI analysis (see Methods, all p-values < 0.05). These results suggest that pRF amplitude sign may structure hippocampal-cortical information flow, in addition to organizing intra-hippocampal perceptual and mnemonic information.

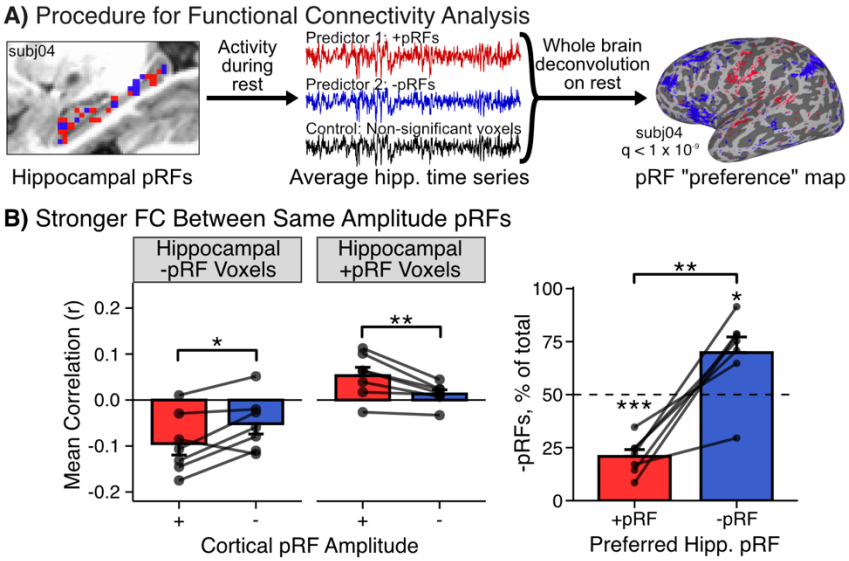

Fig 4. *Hippocampal pRFs demonstrate a functional connectivity preference for cortical pRFs of the same signed amplitude.* ***A.*** *To assess the influence of pRF amplitude sign on hippocampal-cortical functional connectivity, we calculated the average activity during resting-state fixation in +pRFs, -pRFs, and non-significant pRFs. We then ran a whole brain deconvolution with all three average time courses as predictors, with a specific general linear test contrasting hippocampal +pRF against hippocampal -pRFs, producing a whole brain "preference" map.* ***B.*** *Hippocampal pRFs demonstrated a preference for cortical pRFs of the same signed amplitude in two ways. First, using the functional connectivity cortical preference map calculated previously as a mask, we found a significantly greater proportion of -pRF voxels among cortical voxels which preferred hippocampal -pRFs, compared to those preferring hippocampal +pRFs (left; two-sided paired t-test; $t(6) = 6.024$; $p = 0.0009$). Additionally, the proportion of -pRFs among hippocampal +pRF preferring voxels was significantly below 50% (one-sided t-test; $t(6) = -9.1$, $p = 0.00005$), while in hippocampal -pRF preferring voxels it was significantly above 50% ($t(6) = 2.68$; $p = 0.019$). This preference was also represented more generally by increased average correlation between hippocampal and cortical pRFs of the same signed amplitude, compared against mismatched sign (right; one-sided paired t-test; hippocampal -pRFs: $t(6) = -2.81$, $p = 0.015$; hippocampal +pRFs: $t(6) = 3.78$, $p = 0.005$). Error bars indicate standard error around the mean. ***$p < 0.001$ **$p < 0.01$ *$p < 0.05$*

Discussion

In conclusion, we investigated retinotopic coding as a possible mechanism for discriminating between external sensory information and internal mnemonic information in the human hippocampus. In all participants, we found significant retinotopic responses in the hippocampus, roughly evenly split between voxels which showed increased signal during visual stimulation (+pRFs) and voxels with a relative decrease in signal (-pRFs), and these visually responsive voxels had stable features across retinotopic mapping runs. Critically, we demonstrate that the

relationship between retinotopic responses in the hippocampus and those in cerebral cortex is consistent with a whole-brain organization scheme where +pRFs and -pRFs preferentially represent perceptual and mnemonic information, respectively. These results have significant implications for understanding hippocampal function and hippocampal-cortical interactions.

Methods

Overview

We used data made publicly available through the Natural Scenes Dataset (NSD, Allen et al. 2022) which included 8 participants scanned extensively at 7T over the course of several days. The high resolution of the data allowed for detailed explorations of hippocampal activity. Relevant to the present study, each participant completed three runs of sweeping bar retinotopic mapping task and several runs of a resting-state fixation task. Retinotopy and fixation data were minimally preprocessed using manual ICA denoising, and all subsequent analyses were performed in participant-specific volume space. To allow for the identification of negative retinotopic responses, pRF modeling was performed using AFNI's mapping procedure (3dNLfim). We did not regress global signal, and data were left unsmoothed.

Participants and Data Acquisition

Data from the eight participants (ages 19-32) included in the NSD release was used for the current study. One participant (subj03) was excluded from all analyses due to an insufficient amount of resting-state fixation data which passed our quality control criteria (see Quality Control and Preprocessing below). The final set of seven participants had a mean age of 26.1 yr (all right-handed; 5 women) and all had normal or corrected-to-normal visual acuity. All participants provided informed consent for the study.

MRI data was acquired at the Center for Magnetic Resonance Research at the University of Minnesota as described in Allen et al. (2022), and the study was approved by the University of Minnesota institutional review board. Briefly, anatomical scans were acquired using a 3T Siemens Prisma scanner with a 32-channel head coil, including several T_1-weighted magnetization prepared rapid acquisition gradient echo (MPRAGE, voxel size = 0.8 mm^3 isotropic, TR = 2,400 ms, TE = 2.22 ms, flip angle = 8°, in-plane acceleration factor = 2) and T_2-weighted sampling perfection with application-optimized contrasts using different flip angle evolution sequence (SPACE, voxel size = 0.8 mm^3 isotropic, TR = 3,200 ms, TE = 563 ms, in-plane acceleration factor = 2) acquisitions. The remaining data was acquired on a 7T Siemens Magnatom scanner and a single-channel-transmit, 32-channel-receive head coil. Functional data were gradient-echo echo-planar scans (voxel size = 1.8 mm^3 isotropic, TR = 1,600 ms, TE = 22 ms, flip angle = 62°, matrix = 120 x 120, field-of-view = 216 mm x 216 mm), corrected with dual-echo fieldmaps (matched slice prescription to EPI, voxel size = 2.2 mm x 2.2 mm x 3.6 mm TR = 510 ms, TE = 8.16 ms, TE = 9.18 ms). For improved hippocampal segmentation, an additional T_2-weighted turbo-spin echo scan was collected (voxel size = 0.357 mm x 0.357 mm

x 1.5 mm, 56 oblique slices perpendicular to anterior-posterior axis of the hippocampus, TR = 16,000 ms, TE = 53 ms, in-plane acceleration factor = 2).

Task Paradigms

The task for retinotopic mapping was adapted from the Human Connectome Project Retinotopy Dataset (Benson et al. 2018, RETBAR1 and RETBAR2) and consisted of a bar aperture slowly moving across the visual field in multiple directions, revealing objects at multiple scales (i.e. faces, houses, and objects) superimposed on a pink-noise background (Fig. 1A). Both the apertures and textures updated at a rate of 15 Hz, and over the course of each run covered a circular region with a diameter of 8.4°. For each 300 second run, participants were instructed to fixate on a small (0.2° x 0.2°) semi-transparent dot in the center of the screen, and indicate with a button press whenever the color of the dot changed (which occurred every 1-5 sec). Three runs of this task were collected, for a total of 900 seconds of data. Additional wedge/ring runs were also acquired as part of the NSD, but here we consider only the bar stimulus, consistent with other studies characterizing -pRFs (Szinte and Knapen 2020; Klink et al. 2021; Steel et al. 2024).

In all resting-state fixation tasks, participants were instructed to fixate on a small white cross (0.5° x 0.5°) in the center of a gray screen. In each session where fixation tasks were acquired, one run was collected at the beginning of the session, and the other at the end. The first fixation run included no additional instructions. For the second fixation run, participants were instructed to take a deep breath 12 sec into the run, when the fixation cross turned red for 4 sec. Each run of fixation was 300 sec, and between 14 and 34 runs were collected for each participant.

Quality Control and Preprocessing

All data was assessed for quality prior to inclusion in the dataset as described in the original data release (Allen et al. 2022). Because of the sensitivity of resting-state functional connectivity to data quality, particularly motion, we performed additional quality control measures on the fixation data. First, to remove artifacts associated with the instructed deep breath during the second fixation run in each session, we removed the first 25 TRs (40s) of every fixation run, leaving 260 sec (4.25 min) of data. We then assessed the quality of this trimmed data using AFNI's quality control report creation tool (APQC, Taylor et al. 2024). We excluded any individual fixation runs with a maximum displacement of greater than 1.8 mm or a framewise displacement greater than 0.12 mm. Runs with a maximum displacement between 1 mm and 1.8 mm, and a framewise displacement of between 0.1 mm and 0.12 mm were assessed on a case-by-case basis, and excluded if the movement was the result of large shifts (approach similar to Du et al. 2024). After these exclusions, one participant (subj03) had only a single fixation run remaining (4.25 min), and so was excluded from the present study's analyses. The other 7 participants had between 8 and 24 runs (mean: 14, sd: 6.13, 34 - 102 min) of fixation after quality control.

Retinotopy and fixation data were minimally preprocessed, including unwarping and aligning, as described in the NSD data release (Allen et al. 2022). To further denoise the data, we performed a manual ICA classification (Griffanti et al. 2014, 2017; Steel et al. 2021), as automated ICA denoising tools have poor performance on high resolution data like the NSD (Beckers et al. 2023). For each run, the time series was decomposed into independent spatial components along with their associated temporal signal using FSL's melodic ICA (Beckmann and Smith 2004). We then assigned each component to either signal or noise using established criteria in the field (Griffanti et al. 2017). After classification, all the noise components were regressed from the data (fsl_regfit; Griffanti et al. 2014), and the resulting denoised time course was normalized to percent signal change. We did not perform global signal regression (Saad et al. 2012), and all functional data was left unsmoothed.

Population Receptive Field Modeling

For population receptive field (pRF) modeling, we average all three denoised and normalized retinotopy runs together to produce a final retinotopy time series, and ran the AFNI modeling procedure using 3dNLfim as described in Silson et al. (2015). First, we produced a final retinotopy time course by averaging the three identical runs of sweeping bar stimulation. Next, the model calculated 4 million predicted time series based on the timing of the presented sweeping bar (resampled to the temporal resolution of the fMRI acquisition, TR = 1.333s), each corresponding to a simple 2D Gaussian receptive field with a given center position and size. For each voxel, the best of these predicted time series was chosen along with a flexible amplitude scalar using a combination of Simplex and Powell optimization algorithms, minimizing the least-squares error between the acquired retinotopy time series and the amplitude-scaled prediction. Importantly, amplitude here reflects the relative activation/deactivation of a given voxel to visual stimulation of its receptive field.

Reliability and Stability of Hippocampal pRF Modeling

To test the reliability of our pRF mapping estimates in the hippocampus, we ran the above pRF model on the average time course from all of a participant's untrimmed (300s) fixation data which passed quality control, using identical model parameters. Critically, the predicted model time courses were still based on the sweeping bar stimulus, which participants did not see during fixation, producing a null distribution of model parameters absent the modeled visual input. We used this null model to identify an appropriate R^2 cutoff for identifying significant pRF voxels (see Results, Fig. 2). In addition to this null-distribution guided R^2 threshold, we screened out pRFs based model estimates of size (sigma) and eccentricity, guided by the size of the presented stimulus (diameter 8.4 d.v.a., bar width 1.05 d.v.a). Specifically, we excluded any voxels with a size estimate smaller than .42 d.v.a. or larger than 3.78 d.v.a (10% and 90% of the largest possible sigma estimate), as well as voxels with a center eccentricity greater than 3.78 d.v.a. (90% of maximum possible eccentricity).

In addition to testing the reliability of hippocampal pRF fits against a fixation-based null, we also sought to validate the stability of pRF features (amplitude sign and center position) between individual runs of the sweeping bar retinotopy task. To do so, we fit the above pRF model on each individual run of the sweeping bar stimulus, rather than the average, producing three sets of model parameters for each hippocampal voxel. We then applied the voxel-level categorization of significant pRFS and non-significant voxels used for the three-run average pRF model (described above), ensuring that the significance categorization would not differ across runs. To assess center position stability, we calculated for each significant voxel the average Euclidean distance between all three pairings of sweeping bar runs (i.e. run 1 - run 2, run 1 - run 3, and run 2 - run 3). We quantified amplitude sign stability by binarizing voxels according to their amplitude, and calculated a Dice-like coefficient ($coefficient = \frac{3|run1 \cap run2 \cap run3|}{|run1|+|run2|+|run3|}$) across all three runs. Specifically, we produced two coefficients per participant: a positive amplitude value (significant pRFs with positive amplitudes binarized to 1, other significant pRFs set to 0), and a negative amplitude (significant pRFS with negative amplitudes binarized to 1, other significant pRFs set to 0). We calculated the significance of these stability measures in each participant by z-scoring the values derived from only significant pRFs with 5000 additional measures derived from a random sampling of all hippocampal voxels, both significant and non-significant. The sampled voxel and significant-only voxel sizes were the same.

Functional connectivity

We used a resting-state functional connectivity approach to explore how pRF model amplitude predicts hippocampal-cortical interactions. We first averaged the time courses of hippocampal significant +pRFs, -pRFs, and non-significant voxels for each run of fixation (without spatial smoothing), then concatenated all of a participant's average runs to produce a time course for each voxel type. We similarly concatenated the fixation run time courses for every voxel in cerebral cortex. Each cerebral time series was then deconvolved (3dDeconvolve) with the three average hippocampal time series (+pRFs, -pRFs, non-significant) as predictors, followed by a general linear test contrasting the +pRF and -pRF parameters to assess each voxels preference for hippocampal positive or negative pRFs. We used this linear deconvolution to assess mean correlation by taking the square root of the voxel-level R^2, multiplied by the sign of the regression coefficient, to produce a Pearson's r.

Visual Field Coverage

To assess the visual field coverage of hippocampal pRFs, we applied a max-operator approach similar to Silson et al. (2021) and Steel et al. (2024). In each participant, we reconstructed the 2D Gaussian corresponding to each significant pRF, with the amplitude fixed to 1. We refer to values derived from this Gaussian as pRF values. Next, we stored the max pRF value across all significant pRFs with a given amplitude (positive or negative) at each point in the visual field, resulting in a max-operator visual coverage map for each participant. Group-level coverage maps present the average across all participant's max-operator maps.

References

Acharya L, **Aghajan ZM**, **Vuong C**, **Moore JJ**, **Mehta MR**. Causal Influence of Visual Cues on Hippocampal Directional Selectivity. *Cell* 164: 197–207, 2016.

Allen EJ, **St-Yves G**, **Wu Y**, **Breedlove JL**, **Prince JS**, **Dowdle LT**, **Nau M**, **Caron B**, **Pestilli F**, **Charest I**, **Hutchinson JB**, **Naselaris T**, **Kay K**. A massive 7T fMRI dataset to bridge cognitive neuroscience and artificial intelligence. *Nat Neurosci* 25: 116–126, 2022.

Beckers AB, **Drenthen GS**, **Jansen JFA**, **Backes WH**, **Poser BA**, **Keszthelyi D**. Comparing the efficacy of data-driven denoising methods for a multi-echo fMRI acquisition at 7T. *NeuroImage* 280: 120361, 2023.

Beckmann CF, **Smith SM**. Probabilistic independent component analysis for functional magnetic resonance imaging. *IEEE Transactions on Medical Imaging* 23: 137–152, 2004.

Benson NC, **Jamison KW**, **Arcaro MJ**, **Vu AT**, **Glasser MF**, **S. Coalson T**, **Essen DCV**, **Yacoub E**, **Ugurbil K**, **Winawer J**, **Kay K**. The Human Connectome Project 7 Tesla retinotopy dataset: Description and population receptive field analysis. *Journal of Vision* 18: 23–23, 2018.

Biswal B, **Zerrin Yetkin F**, **Haughton VM**, **Hyde JS**. Functional connectivity in the motor cortex of resting human brain using echo-planar MRI. *Magn Reson Med* 34: 537–541, 1995.

Cohen NJ, **Squire LR**. Preserved Learning and Retention of Pattern-Analyzing Skill in Amnesia: Dissociation of Knowing How and Knowing that. *Science* 210: 207–210, 1980.

Cox RW. AFNI: software for analysis and visualization of functional magnetic resonance neuroimages. *Comput Biomed Res* 29: 162–173, 1996.

Cox RW. AFNI: What a long strange trip it's been. *Neuroimage* 62: 743–747, 2012.

Du J, **DiNicola LM**, **Angeli PA**, **Saadon-Grosman N**, **Sun W**, **Kaiser S**, **Ladopoulou J**, **Xue A**, **Yeo BTT**, **Eldaief MC**, **Buckner RL**. Organization of the human cerebral cortex estimated within individuals: Networks, global topography, and function. *J Neurophysiol* , 2024. doi:10.1152/jn.00308.2023.

Dumoulin SO, **Wandell BA**. Population receptive field estimates in human visual cortex. *NeuroImage* 39: 647–660, 2008.

Epstein R, **Kanwisher N**. A cortical representation of the local visual environment. *Nature* 392: 598–601, 1998.

Felleman DJ, **Van Essen DC**. Distributed Hierarchical Processing in the Primate Cerebral Cortex. *Cerebral Cortex* 1: 1–47, 1991.

Fox MD, **Raichle ME**. Spontaneous fluctuations in brain activity observed with functional magnetic resonance imaging. *Nat Rev Neurosci* 8: 700–711, 2007.

Griffanti L, **Douaud G**, **Bijsterbosch J**, **Evangelisti S**, **Alfaro-Almagro F**, **Glasser MF**, **Duff EP**, **Fitzgibbon S**, **Westphal R**, **Carone D**, **Beckmann CF**, **Smith SM**. Hand classification of fMRI ICA noise components. *NeuroImage* 154: 188–205, 2017.

Griffanti L, **Salimi-Khorshidi G**, **Beckmann CF**, **Auerbach EJ**, **Douaud G**, **Sexton CE**, **Zsoldos E**, **Ebmeier KP**, **Filippini N**, **Mackay CE**, **Moeller S**, **Xu J**, **Yacoub E**, **Baselli G**, **Ugurbil K**, **Miller KL**, **Smith SM**. ICA-based artefact removal and accelerated fMRI acquisition for improved resting state network imaging. *NeuroImage* 95: 232–247, 2014.

Gulli RA, **Duong LR**, **Corrigan BW**, **Doucet G**, **Williams S**, **Fusi S**, **Martinez-Trujillo JC**. Context-dependent representations of objects and space in the primate hippocampus during virtual navigation. *Nat Neurosci* 23: 103–112, 2020.

Klink PC, **Chen X**, **Vanduffel W**, **Roelfsema PR**. Population receptive fields in nonhuman primates from whole-brain fMRI and large-scale neurophysiology in visual cortex. *eLife* 10: e67304, 2021.

Knapen T. Topographic connectivity reveals task-dependent retinotopic processing throughout the human brain. *Proceedings of the National Academy of Sciences* 118: e2017032118, 2021.

O'Keefe J, **Dostrovsky J**. The hippocampus as a spatial map. Preliminary evidence from unit activity in the freely-moving rat. *Brain Res* 34: 171–175, 1971.

Purandare CS, **Dhingra S**, **Rios R**, **Vuong C**, **To T**, **Hachisuka A**, **Choudhary K**, **Mehta MR**. Moving bar of light evokes vectorial spatial selectivity in the immobile rat hippocampus. *Nature* 602: 461–467, 2022.

Saad ZS, **Gotts SJ**, **Murphy K**, **Chen G**, **Jo HJ**, **Martin A**, **Cox RW**. Trouble at Rest: How Correlation Patterns and Group Differences Become Distorted After Global Signal Regression. *Brain Connectivity* 2: 25–32, 2012.

Scoville WB, **Milner B**. Loss of recent memory after bilateral hippocampal lesions. *J Neurol Neurosurg Psychiatry* 20: 11–21, 1957.

Silson EH, **Chan AW-Y**, **Reynolds RC**, **Kravitz DJ**, **Baker CI**. A Retinotopic Basis for the Division of High-Level Scene Processing between Lateral and Ventral Human Occipitotemporal Cortex. *J Neurosci* 35: 11921–11935, 2015.

Silson EH, **Zeidman P**, **Knapen T**, **Baker CI**. Representation of Contralateral Visual Space in the Human Hippocampus. *J Neurosci* 41: 2382–2392, 2021.

Steel A, **Robertson CE**, **Taube JS**. Current Promises and Limitations of Combined Virtual Reality and Functional Magnetic Resonance Imaging Research in Humans: A Commentary on Huffman and Ekstrom (2019). *Journal of Cognitive Neuroscience* 33: 159–166, 2021.

Steel A, **Silson EH**, **Garcia BD**, **Robertson CE**. A retinotopic code structures the interaction between perception and memory systems. *Nat Neurosci* 27: 339–347, 2024.

Szinte M, **Knapen T**. Visual Organization of the Default Network. *Cerebral Cortex* 30: 3518–3527, 2020.

Taylor PA, **Glen DR**, **Chen G**, **Cox RW**, **Hanayik T**, **Rorden C**, **Nielson DM**, **Rajendra JK**, **Reynolds RC**. A Set of FMRI Quality Control Tools in AFNI: Systematic, in-depth and interactive QC with afni_proc.py and more. *bioRxiv* 2024.03.27.586976, 2024.

Supplemental Materials

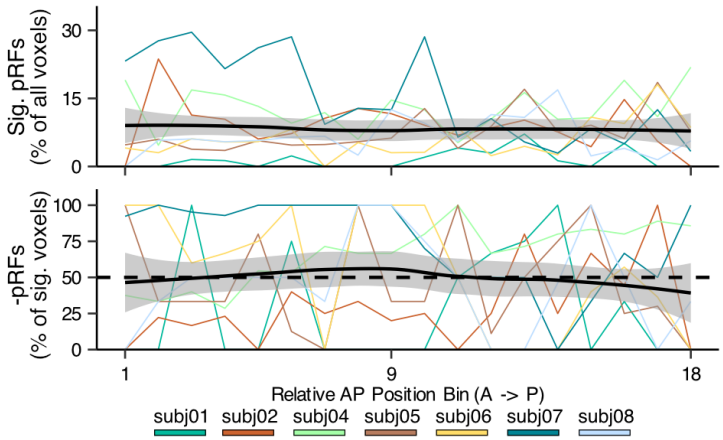

Supplemental Fig 1. *Hippocampal pRFs are evenly distributed along the long axis. The proportion of significant pRFs (top) or -pRFs among significant pRFs (bottom) calculated in 18 bins evenly spaced along the hippocampal long axis. Mean across participants is indicated by the solid black line, shading indicated standard error around the mean. To establish significant differences along the long axis we used a linear mixed-effects model with a random intercept for subject (proportion ~ AP bin + (1|subject). This demonstrated that neither the proportion of significant pRFs (F(1, 118) = 0.608; p = 0.437) nor the proportion of -pRFs (F(1,118) = 0.469, p = 0.495) significantly differed along the long axis.*

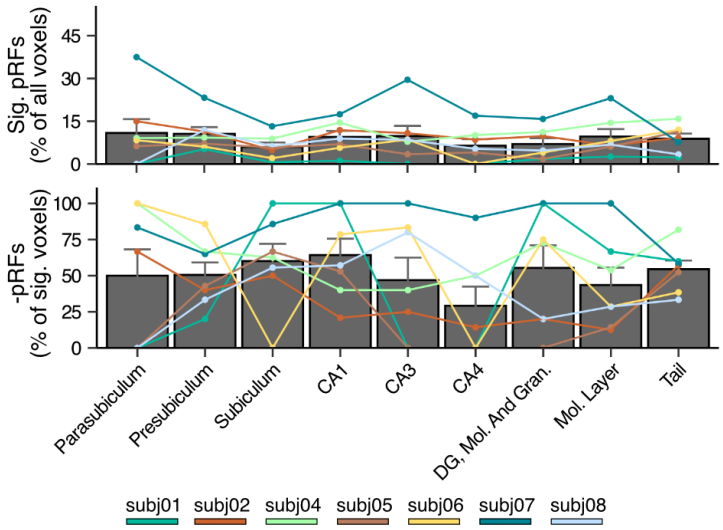

Supplemental Fig 2. *Hippocampal pRFs are evenly distributed among subfields. The proportion of significant pRFs (top) or -pRFs among significant pRFs (bottom) calculated in hippocampal subfield regions automatically generated through Freesurfer. Bars indicate mean across participants, error bar is standard error of that mean. To establish significant differences we used a linear mixed-effects model with a random intercept for subject (proportion ~ subfield + (1|subject). This demonstrated that neither the proportion of significant pRFs ($F(8, 48) = 1.268$; $p = 0.282$) nor the proportion of -pRFs ($F(8,48) = 0.853$, $p = 0.562$)) significantly differed significantly between subfields.*

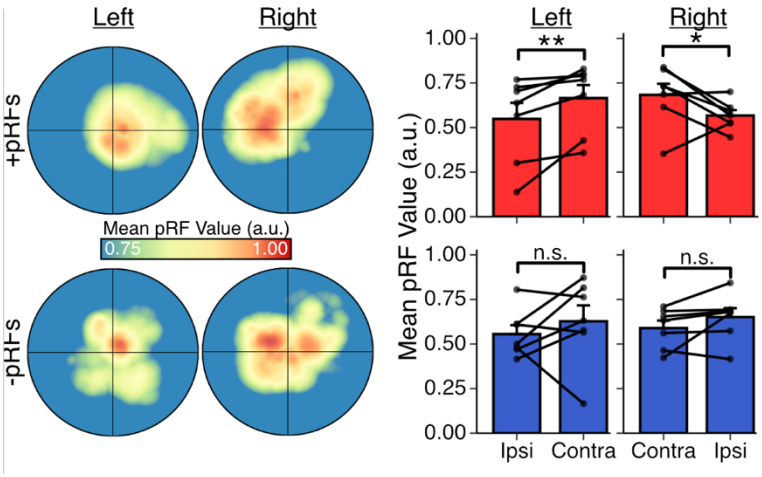

Supplemental Fig 3. *Hippocampal -pRFs deviate from +pRF visual hemi-field preference. We found that hippocampal +pRFs preferentially cover the contralateral visual field (top; one-sided paired t-test, H_a: $\mu_{contra} > \mu_{ipsi}$; left hemisphere: $t(6) = -3.256$, $p = 0.008$; right hemisphere: $t(6) = -1.972$; $p = 0.048$), as previously reported by Silson et al. (2021). In contrast, -pRFs did not show a statistically significant bias for the contralateral hemifield (bottom; left hemisphere: $t(6) = 0.863$, $p = 0.21$; right hemisphere: $t(6) = 1.648$; $p = 0.925$).*

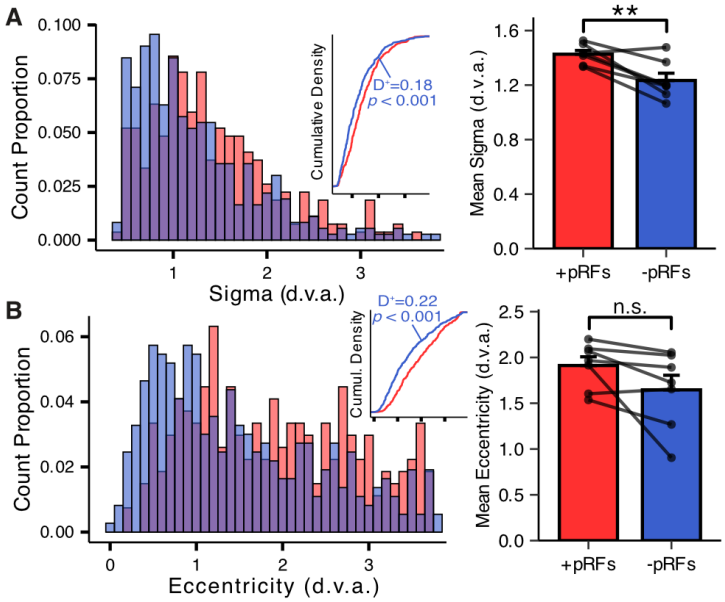

Supplemental Fig 4. *Compared to hippocampal +pRFs, -pRFs are smaller and less eccentric. Plots comparing the size (A) and eccentricity (B) of significant positive and negative pRFS in the hippocampus. In both a distribution pooled across participants (left) and on the participant-level (right), -pRFs demonstrated a significantly smaller size than +pRFs (pooled statistic: asymptotic two-sample Kolmogorov-Smirnov test; participant-level statistic: two-sided paired t-test, t(6) = -3.981, p = 0.007). Negative pRFs were also significantly less eccentric in the pooled distributions, but this effect was not significant on the participant level (p = 0.094)*

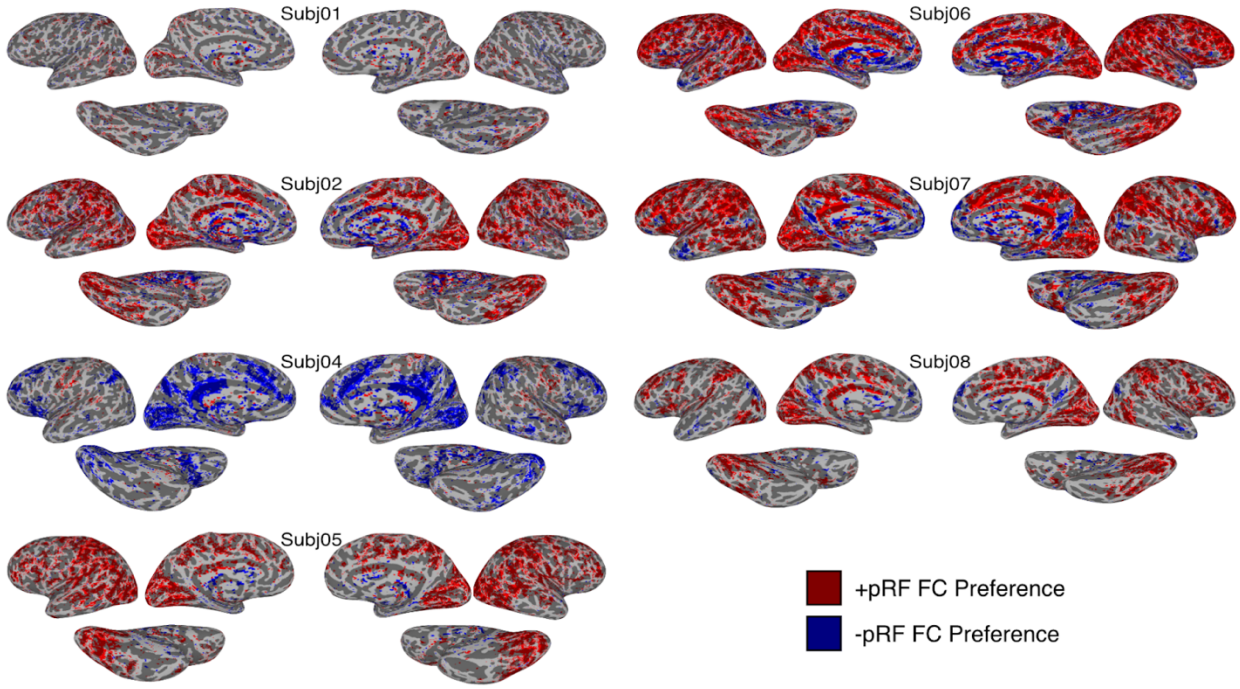

Supplemental Fig 5. *Hippocampus-cortex functional connectivity preference maps for all participants.*

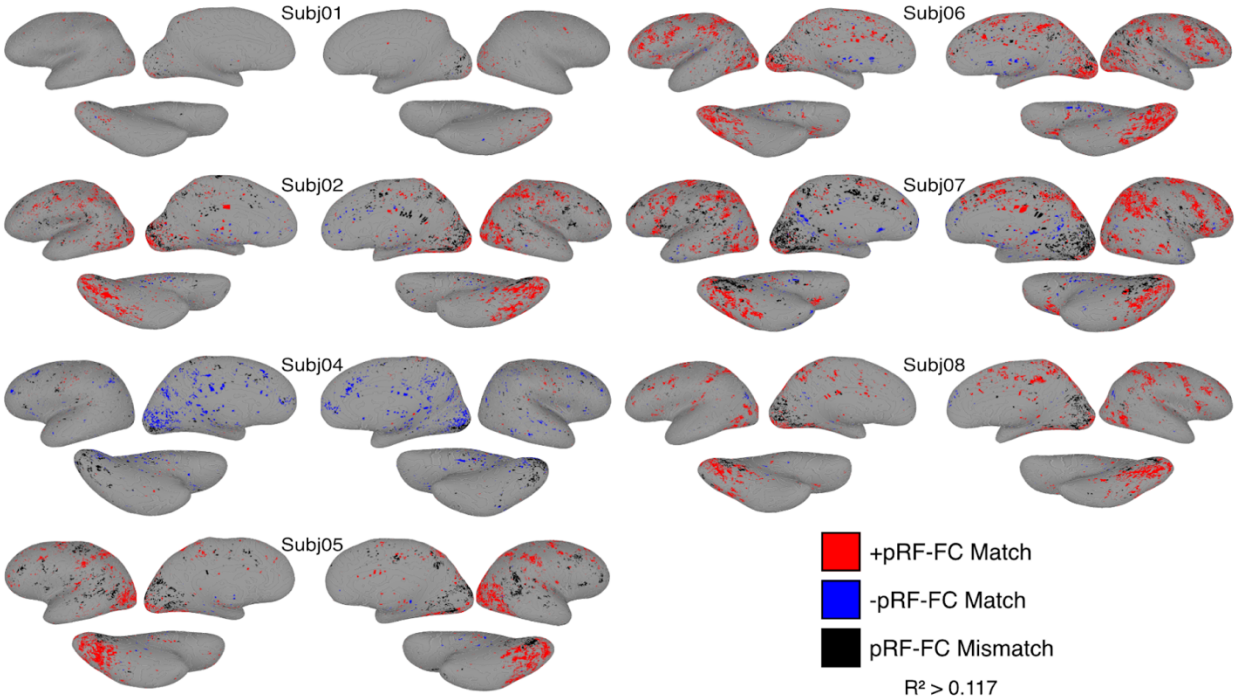

Supplemental Fig 6. *Convergence of hippocampus-cortex FC preference maps with cortical pRF amplitudes. Red colors indicate cortical +pRFs within regions of cortex preferring hippocampal +pRFs, and similarly blue for -pRFs. Black indicates a mismatch between FC preference and pRF amplitude, either -pRF preference with a +pRF, or vice versa.*